Question 1

a.

The eddy-uv case is a special case of solutions to the 2D incompressible NS equations (the NS momentum equation is reproduced below)

$$\rho\left(\frac{\partial u_i}{\partial t} + u_j\frac{\partial u_i}{\partial x_j}\right) = -\frac{\partial p}{\partial x_i} + \mu\frac{\partial^2 u_i}{\partial x_j\,\partial x_j} + f_i$$

The solution is an artificial solution on a double periodic domain (ie, period in x and in y). The initial conditions and solution are composed of a series of eigenfunctions making up a series. The nature of the solution allows for a closed-form solution across time, which is a rarity (closed-form transient solutions to NS are not common). Comparing the SEM solution to the analytical solution allows verification of the code.

b.

Both solutions, at Re=20 and Re=100, were run for 2000 timesteps at dt=1e-4s, for a total of 0.2s of simulated time. Both solutions were run with 15th-order elements.

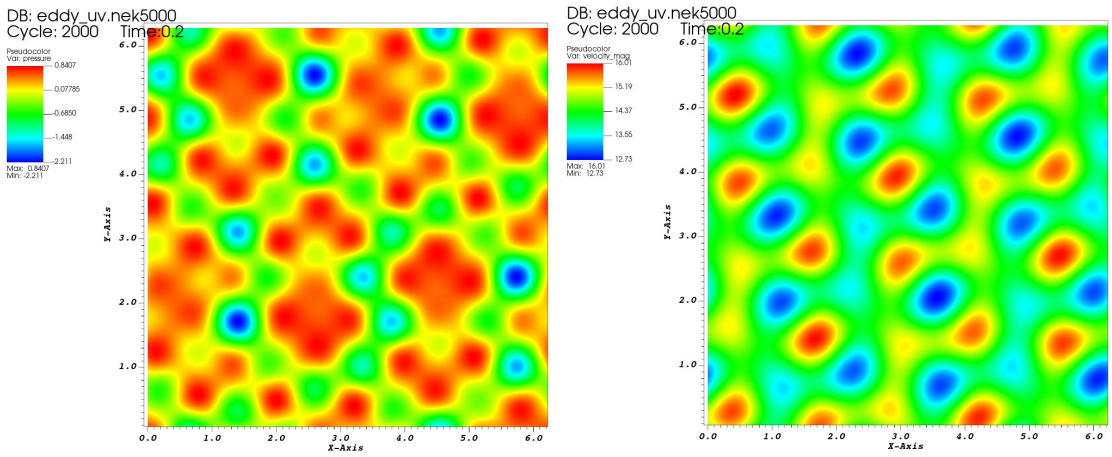

Figure 1: Pressure and velocity snapshot at Re=20

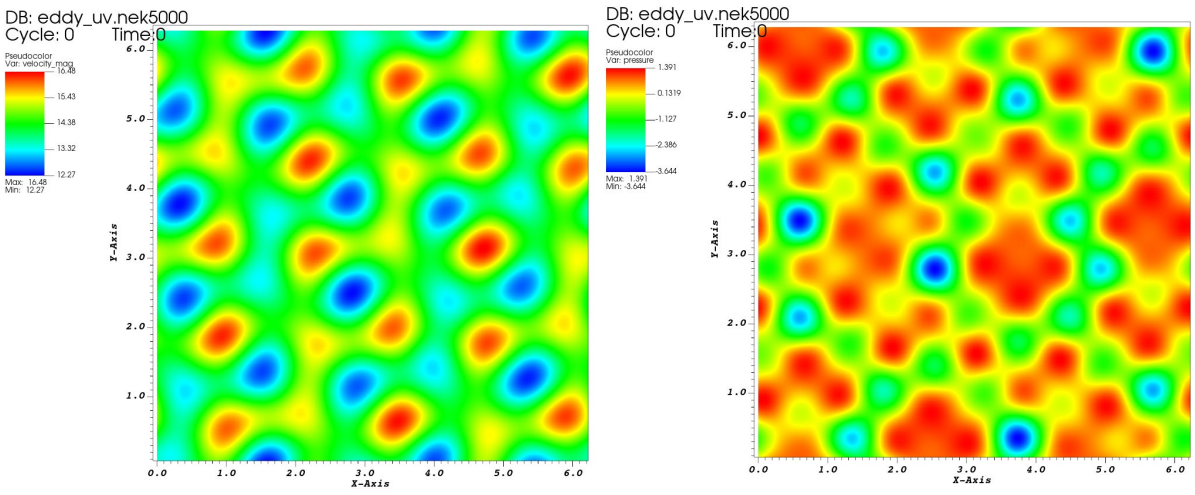

Figure 2: Pressure and velocity snapshot at Re=100

The only visible difference between the two solutions is the magnitude of the solution. Plotting a glyph of the velocity shows the eddies:

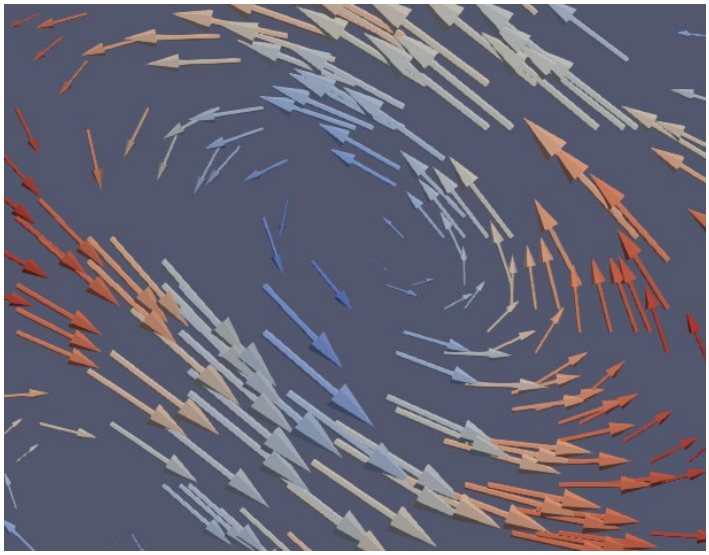

Figure 3: Velocity glyph

The velocity and pressure fields advect up and to the right, and they are maintained in a coherent manner. The difference is marginal between the two cases at Re=20 and Re=100, but at low Reynolds numbers the vortices would be expected to diffuse more. As they advect to the top and right, they reappear at the bottom left, in accordance with the doubly-periodic boundary condition.

C.

The error with the initial parameters and Re=100 is quite large. It is plotted below in Fig. 4.

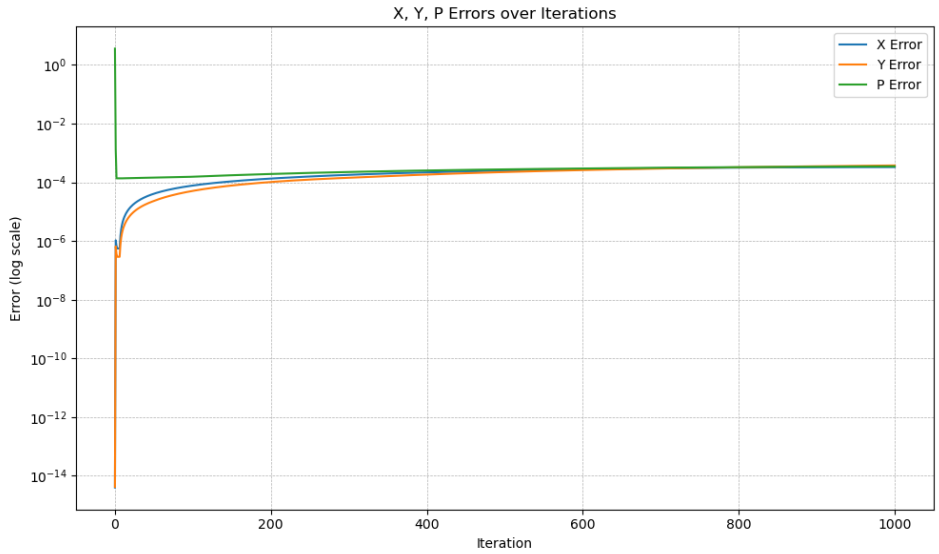

Figure 4: Error with initial case setup

Changing the polynomial order to 15 and the timestep to 1e-5 (from 1e-4) results in much lower error against the analytical solution. The error is on the order of 1e-12 for the x- and y- error, which is not far off double machine precision (1e-16).

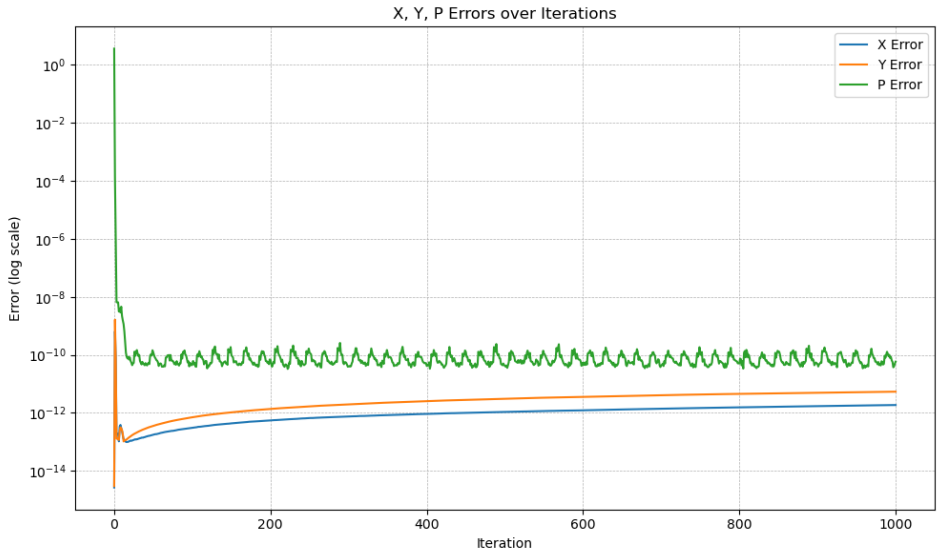

Figure 5: Error with modified case setup

d.

The error in the simulation results from truncation errors and round-off errors. There is a finite threshold for how low the error can be driven. Truncation error is decreased by using higher-order polynomials or more elements (which are both equivalent to adding degrees of freedom). Roundoff error is a necessary evil with floating-point computing. It could be driven by using quad arithmetic instead of double arithmetic but the cost is most likely not worth it.

Question 2

a.

This is the typical external flow past a cylinder problem. Once again, the PDE in question is the incompressible NS:

$$\rho\left(\frac{\partial u_i}{\partial t} + u_j\frac{\partial u_i}{\partial x_j}\right) = -\frac{\partial p}{\partial x_i} + \mu\frac{\partial^2 u_i}{\partial x_j\,\partial x_j} + f_i$$

A cylinder is simulated inside a uniform left-to-right flow. The boundary condition is no-slip and no-penetration along the cylinder surface. The top and bottom boundary conditions are flow-through, the left boundary condition is an inflow, and the right boundary condition is an outflow.

b.

Below, the velocity magnitude at the final iteration is plotted for various Reynolds numbers.

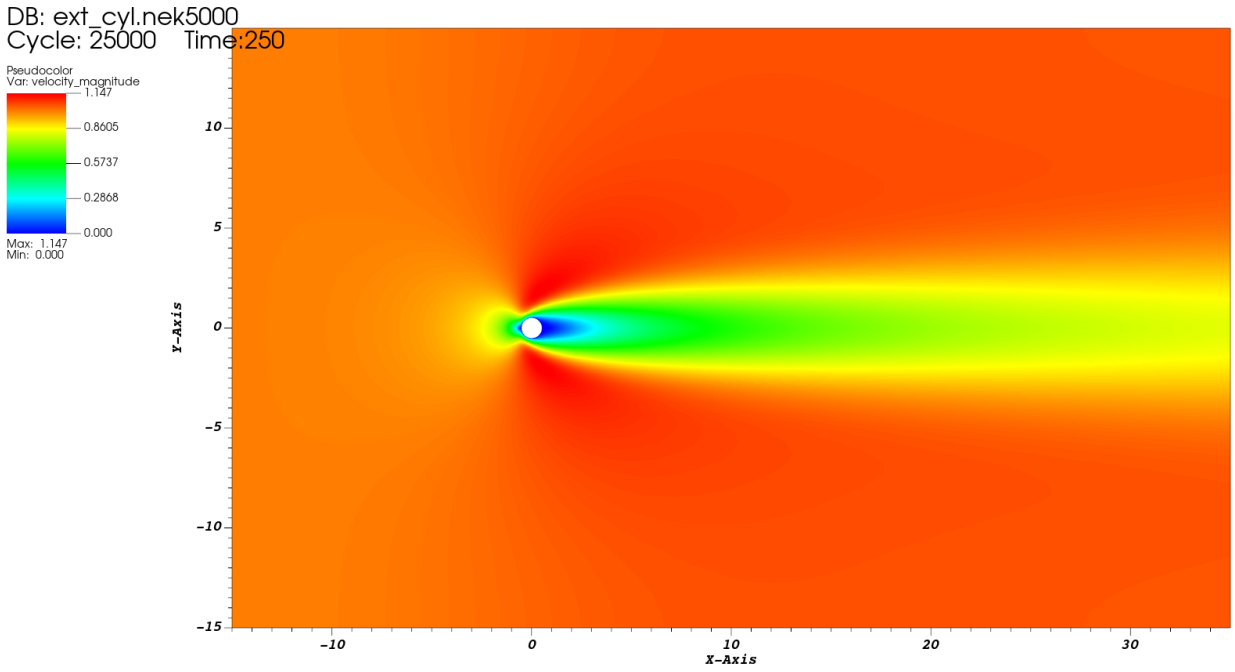

Figure 6: External cylinder flow at Re=10. The wake is very wide and no oscillations or vortex-shedding is observed.

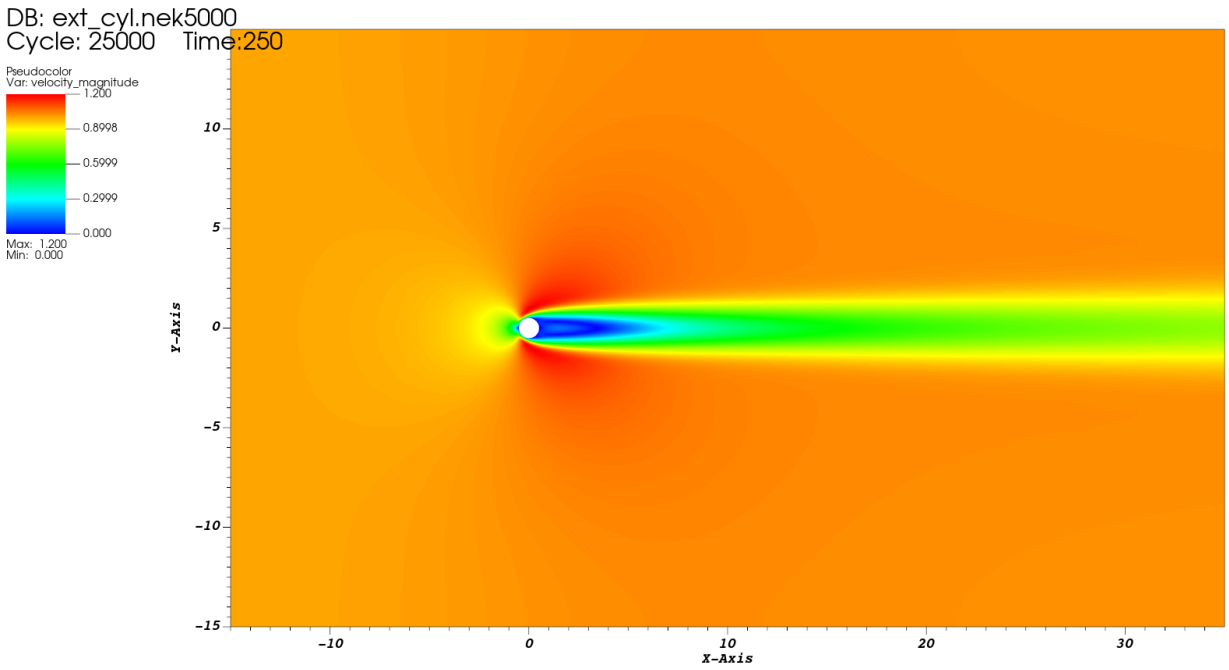

Figure 7: External cylinder flow at Re=50. The wake is stronger, longer, and thinner, but still no oscillations or vortex-shedding is observed.

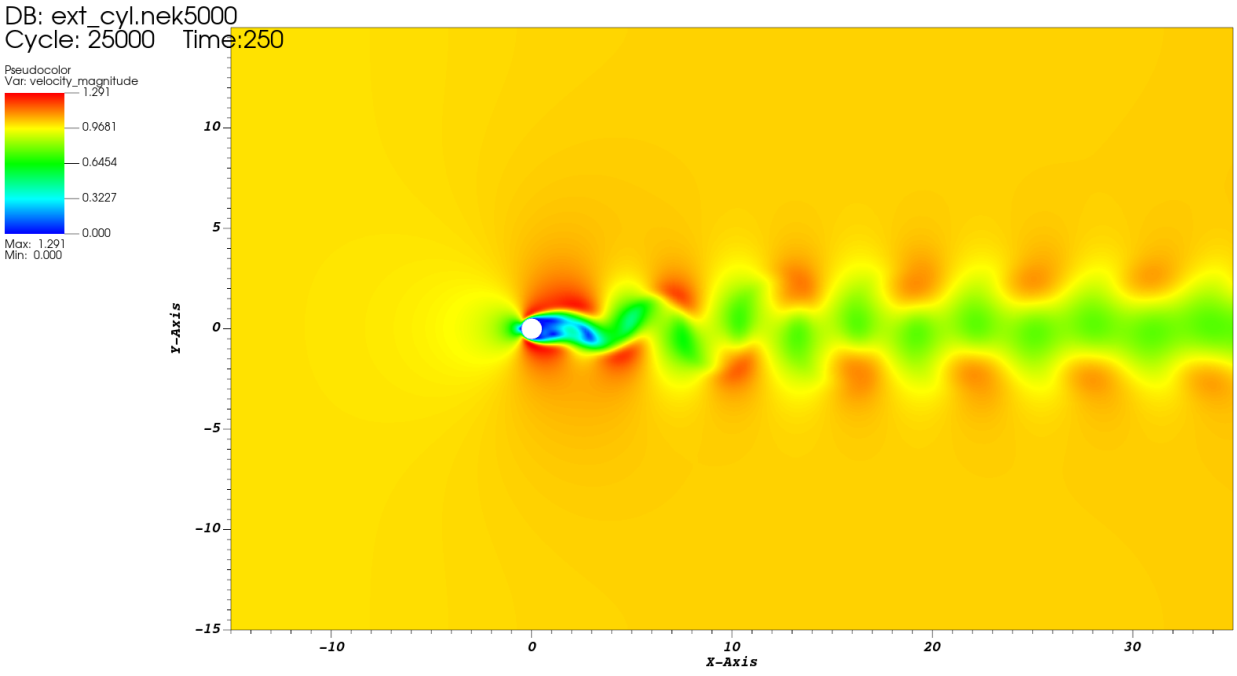

Figure 8: External cylinder flow at Re=75. Vortex shedding has begun.

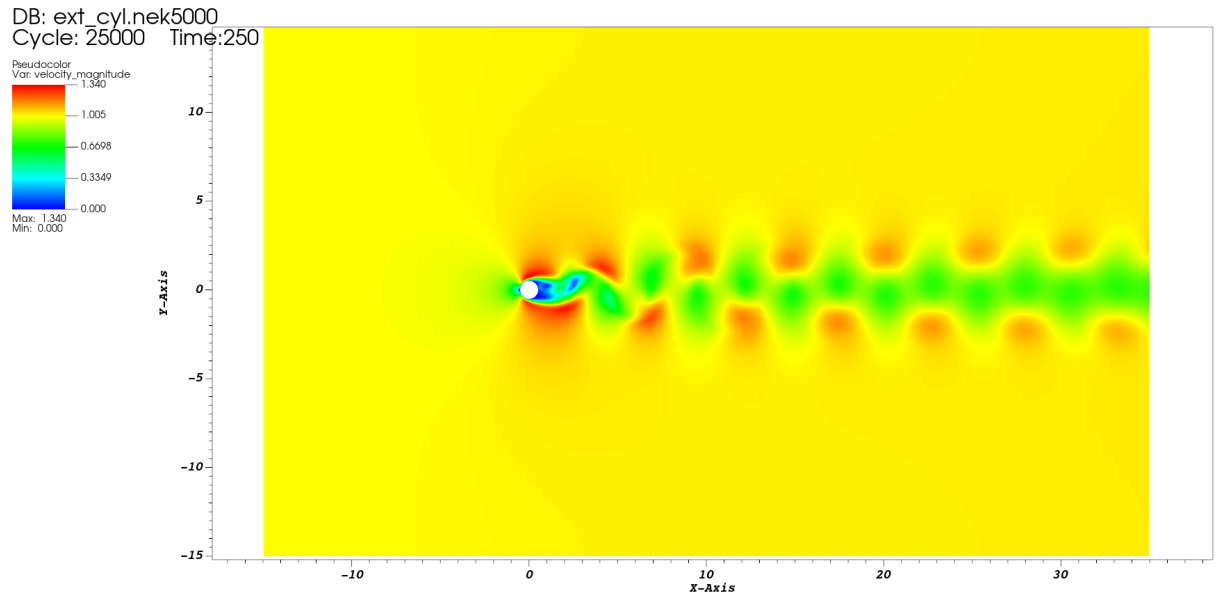

Figure 6: External cylinder flow at Re=100. The shed vortices appear smaller and at higher frequency than at Re=75

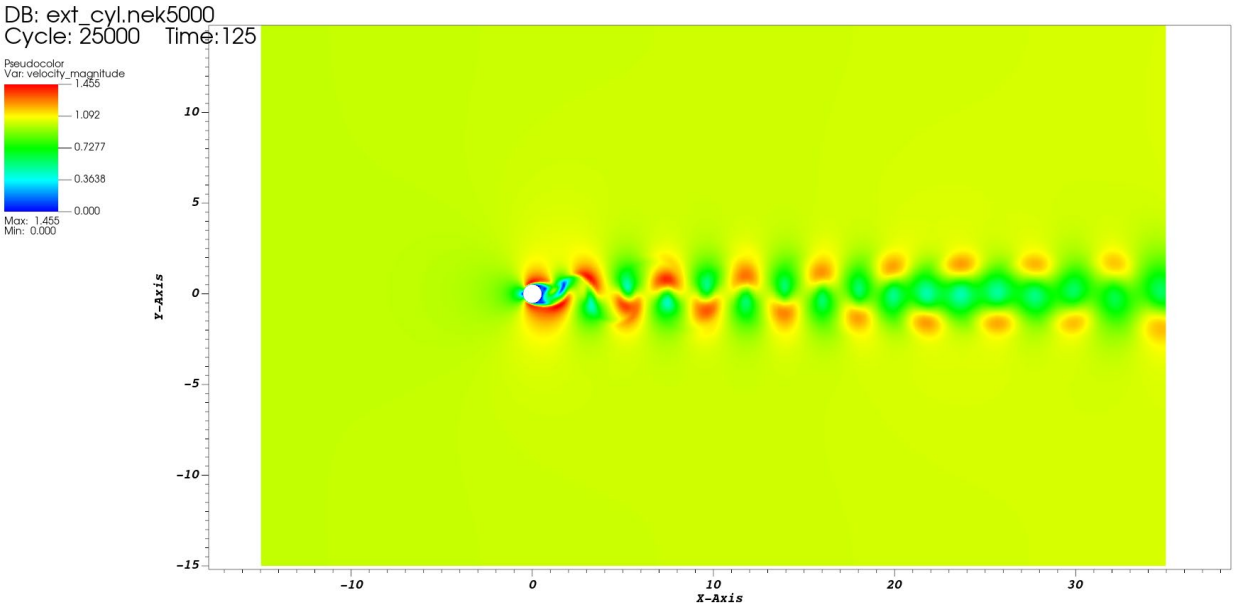

Figure 8: External cylinder flow at Re=250. The shed vortices are much smaller and higher frequency.

Based on this range of cases, I expect that vortex shedding in this flow begins at a Reynolds number between 50-75. This aligns with the literature, which generally highlights Re~50-60 as the point where vortex shedding begins around a bluff body in a 2D flow.

C.

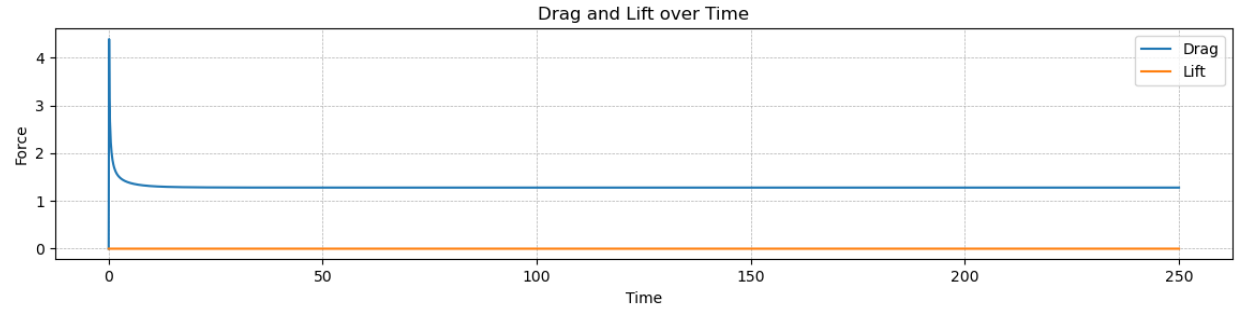

Figure 9: Drag and lift over time at Re=10

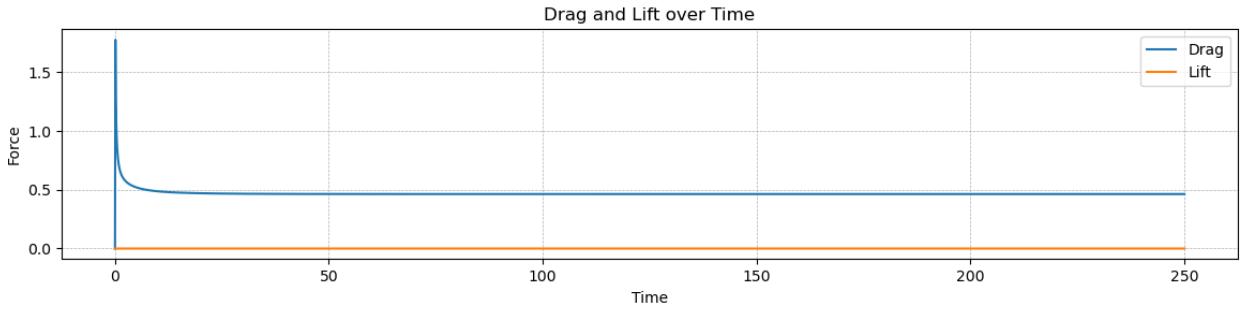

Figure 10: Drag and lift over time at Re=50

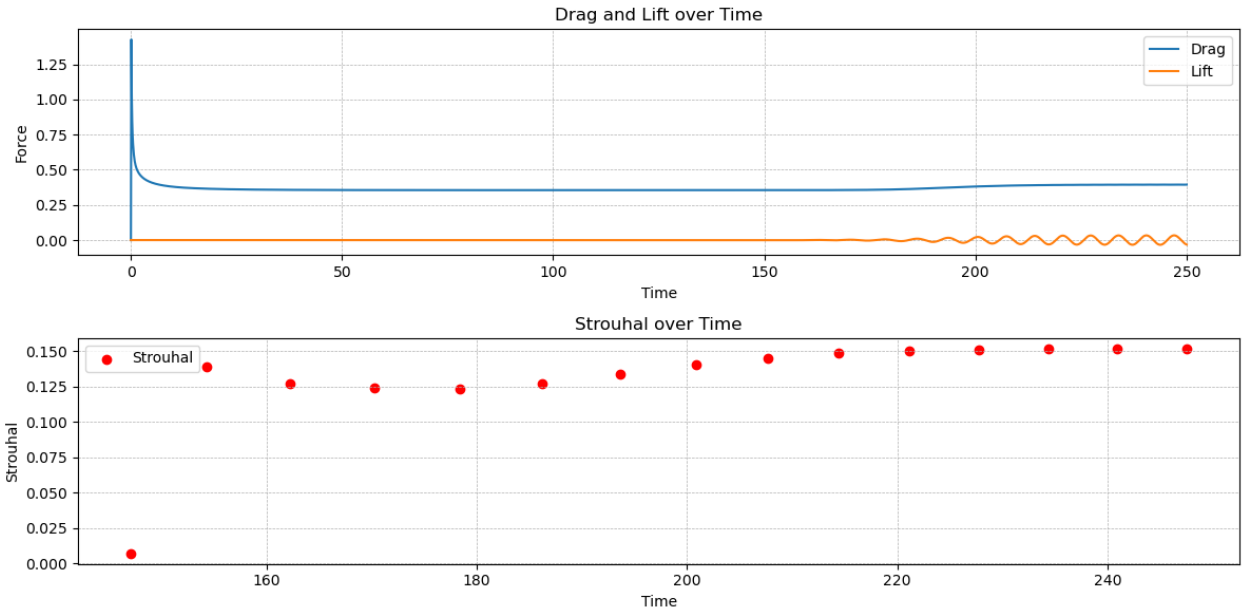

Figure 11: Drag and lift over time at Re=75

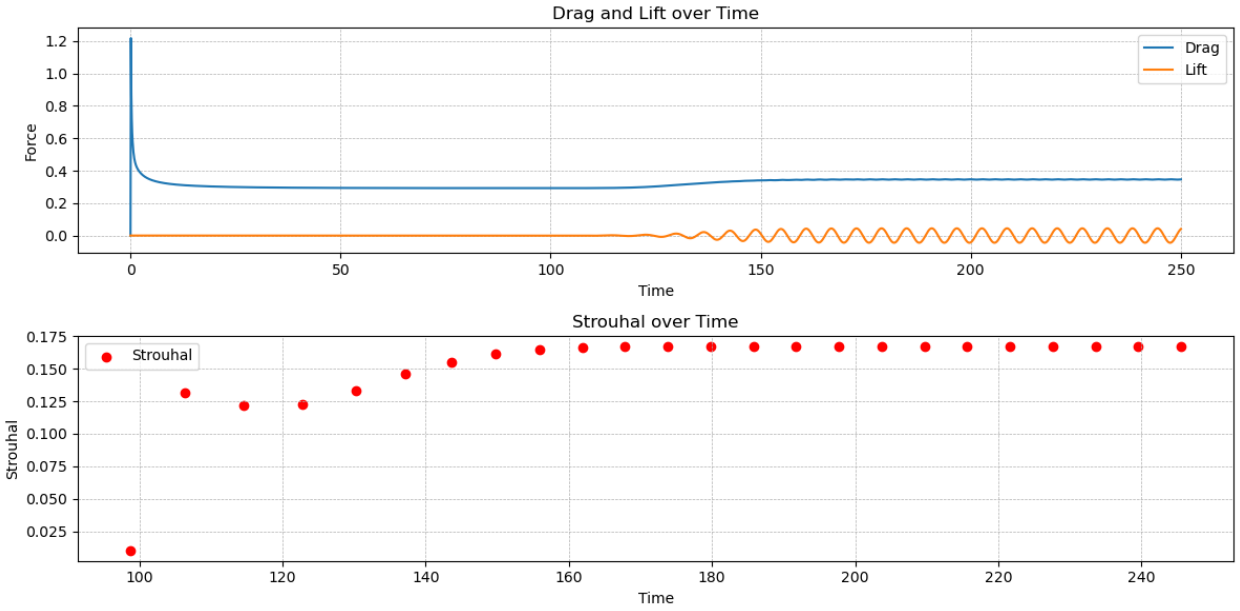

Figure 12: Drag and lift over time at Re=100

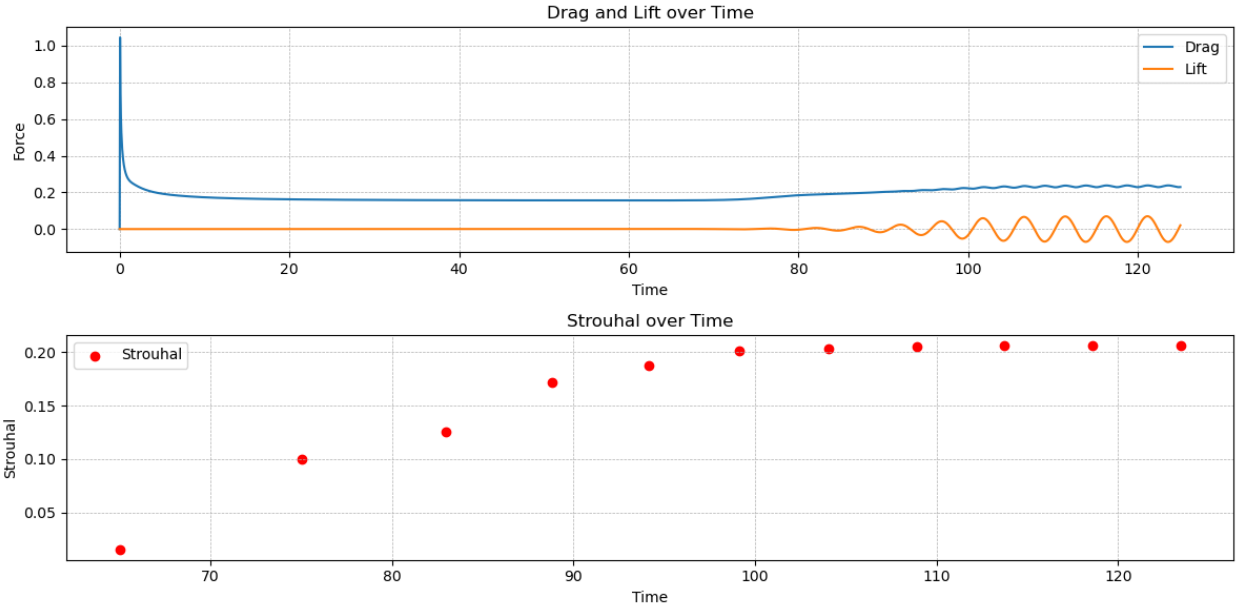

Figure 13: Drag and lift over time at Re=10

The drag and lift for all the cases, as well as the Strouhal number for cases Re>75 where vortex shedding is observed, is plotted above. The behavior aligns with the behaviors observed in full plots of the solution for part b.

The steady, time averaged values for lift, drag, and Strouhal number are plotted below.

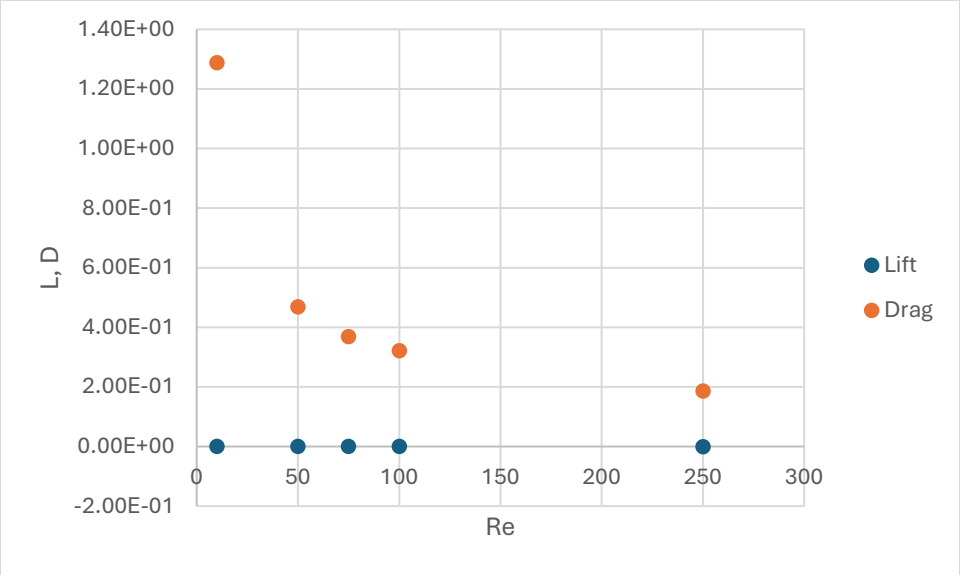

Figure 14: Steady values for lift and drag

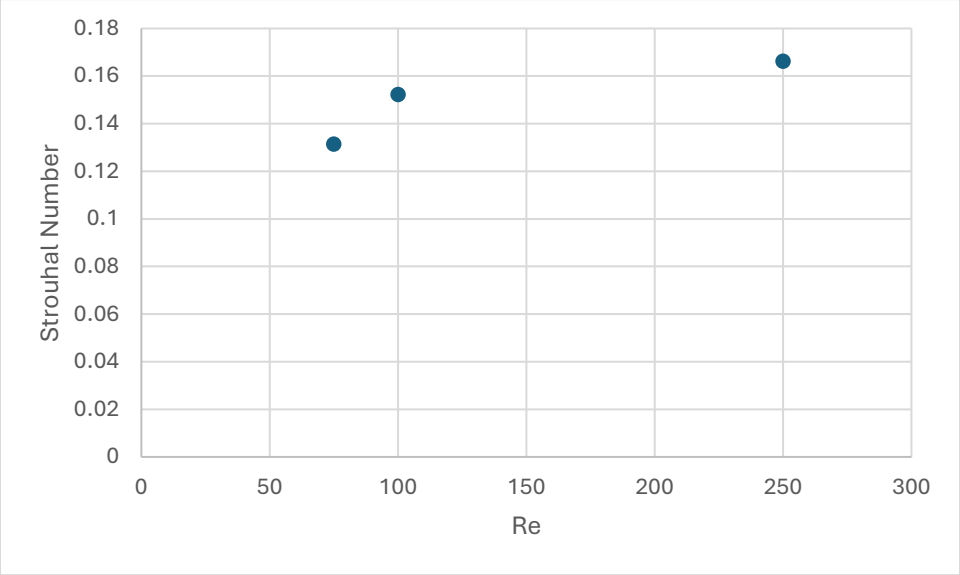

Figure 15: Steady value for Strouhal number

As expected, the lift on a non-rotating cylinder is 0. Drag decreases with Reynolds number, which is generally observed for spheres and cylinders. The Strouhal number increases with Re, although firm conclusions about the Strouhal number are difficult to make with only 3 data points.

d.

To prove grid convergence, the Re=250 case was run again with 12th-order GLL elements. This necessitated a decrease in the timestep to 2.5e-4. Grid convergence is evaluated by plotting the lift and drag against the lift and drag for the 6th-order element case.

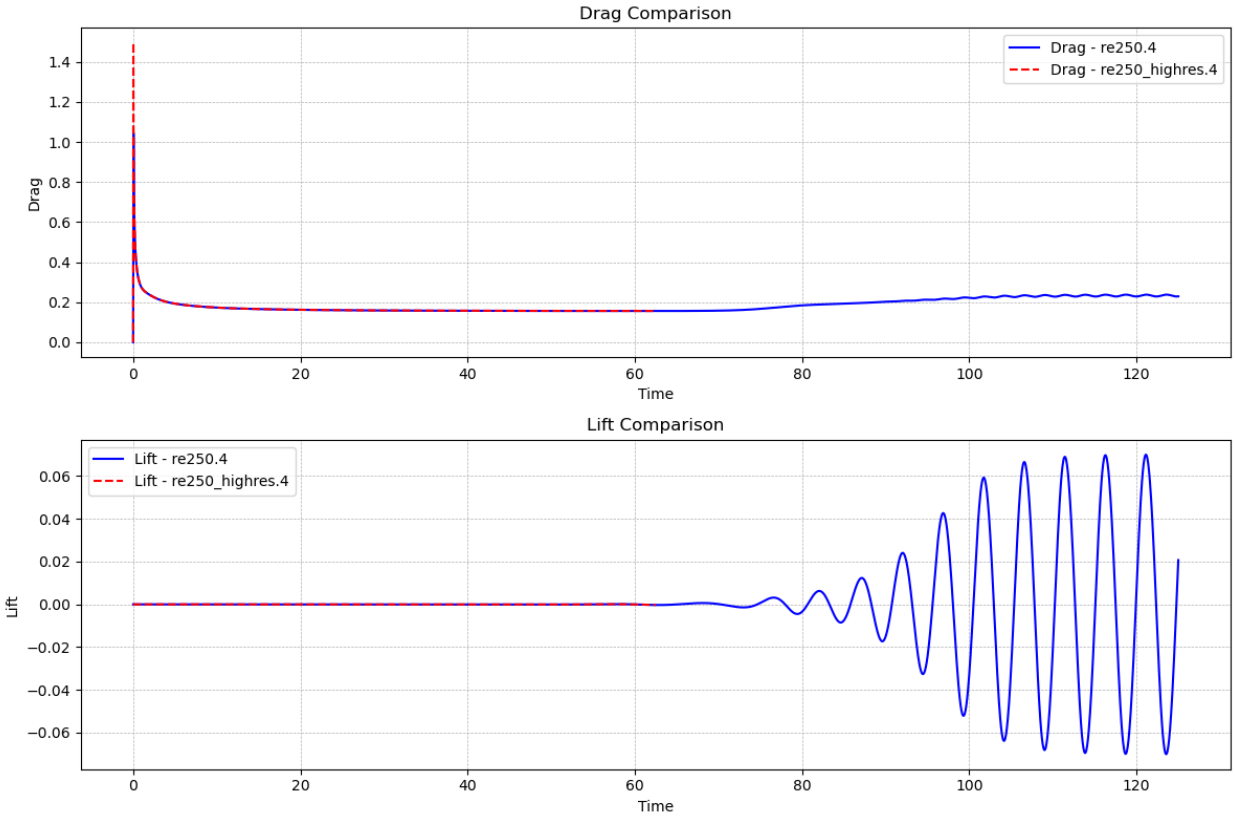

Agreement is observed, indicating that grid convergence has been reached. Due to the smaller timestep, only half of the time was simulated in the high-resolution case (I didn't have time to run the high-res case on my machine before turning this in). So, the indication of grid convergence is not definitive.

Final Project Description

Spencer Adams, Logan Freeman, and Nathan Hoch
Utah State University, Logan, UT, 84321

I. Project Outline

Project Objectives

Develop a basic 2D SEM code with the following capabilities:

- Read in or generate a quad mesh
- Generate Gauss-Lobatto-Legendre (GLL) points and weights for each element
- Assemble stiffness and mass matrices
- Solve the linear system with existing solvers
- Compare to special analytic cases

II. Toy Problems

Numerical methods are generally developed and tested against small-scale toy problems before moving on to solving the PDEs of interest. Toy problems exhibit similar characteristics, but are simpler. In addition, toy problems with closed-form solutions are used to validate numerical solution techniques. We will work towards a Navier-Stokes SEM solver by first solving the 1D wave equation and 1D heat equation.

A. Advection Equation

The advection equation is a linear, first-order PDE with a hyperbolic character. This equation is a good surrogate for the advection term of the Navier-Stokes equation. Using the SEM method, we will solve the wave equation on a periodic domain:

$$u_t = cu_x,\ u(x,0) = u_0(x),\ u(0,t) = u(L,t),\ 0 < x < L \tag{1}$$

Results will be compared to simple finite-difference techniques of low- and high-order, and the dispersion and dissipation error will be quantified against the known exact solution:

$$u(x,t) = u_0(x - ct) \tag{2}$$

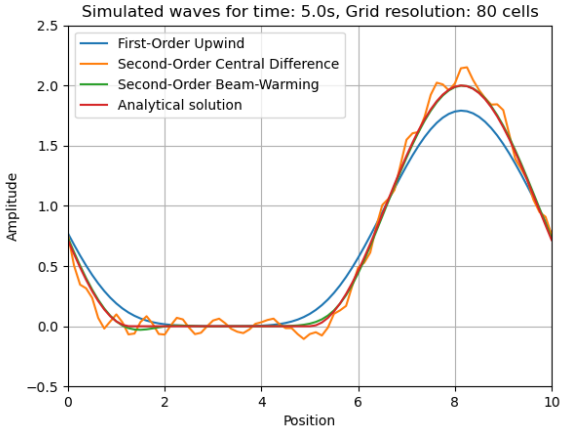

Fig. 1 Figure 1: Numerical dispersion and dissipation evident in finite-difference solutions to 1D advection equation with various schemes. Displayed results are from a code written by Freeman for MAE 5440.

The spectral element method will out-perform finite difference methods in terms of numerical dispersion and dissipation.

B. Heat Equation

The heat equation is a linear, second-order PDE with a parabolic character. It is a good surrogate for the diffusive viscous term in the Navier-Stokes equation. Using SEM, we will solve the 1D heat equation on a finite domain with Neumann boundary conditions:

$$u_t = \alpha u_{xx},\ u(x,0) = u_0(x),\ u_x(0,t) = g_0,\ u_x(L,t) = g_L,\ 0 < x < L \tag{3}$$

This problem has a closed-form solution, and so comparisons can be made between the analytical and SEM solution. Once again, SEM results will be compared to finite-difference results.

III. Non-dimensionalized Navier-Stokes

The main PDE system which will be solved in this project is the incompressible Navier-Stokes equations. In tensor notation, these are

$$\frac{\partial u_i}{\partial x_i} = 0 \tag{4}$$

$$\frac{\partial u_i}{\partial t} + u_j \frac{\partial u_i}{\partial x_j} = -\frac{1}{\rho}\frac{\partial p}{\partial x_i} + \nu \frac{\partial^2 u_i}{\partial x_j \partial x_j} \tag{5}$$

where the body force of gravity has been included in the pressure term as a hydrostatic pressure.

The equations can be non-dimensionalized with reference length L and reference velocity u_∞ which leads to the forms:

$$\frac{\partial u_i^*}{\partial x_i^*} = 0 \tag{6}$$

and

$$\frac{\partial u_i^*}{\partial t^*} + u_j^* \frac{\partial u_i^*}{\partial x_j^*} = -\frac{\partial p^*}{\partial x_i^*} + \frac{1}{\mathrm{Re}} \frac{\partial^2 u_i^*}{\partial x_j^* \partial x_j^*} \tag{7}$$

where Re is defined as:

$$\mathrm{Re} = \frac{u_\infty L}{\nu} \tag{8}$$

Varying the Reynolds number allows for different behavior of the PDE system. At high Reynolds numbers, fluid flows exhibit turbulence as the damping effect of the diffusive term diminishes. This project will not attempt to model or simulate scale-resolved turbulence, instead focusing on establishing a functioning SEM solver for simple flows.

IV. Current High-Level Understanding of SEM

This section presents our current high-level understanding of a 2D SEM. We will attempt to explained the main ideas in our own words. This exercise is a relevant part of the final project description our objective is to implement a basic 2D SEM code.

For a given 2D flow problem governed by the Navier-Stokes equation (Eq. (7)), the spectral element method results in a continuous solution of u at any point in the domain. The domain is first broken up into 4-sided elements (a quad mesh). Each element is then mapped to another plane where the element is perfectly square and the x, and y bounds are both $[-1, 1]$.

The velocity $\boldsymbol{u}$ at any point within an element Ω^e is

$$\boldsymbol{u}(\mathbf{x})|_{\Omega^e} = \boldsymbol{u}^e(\mathbf{r}) = \sum_{i=0}^{N}\sum_{j=0}^{N} l_i(r) l_j(s) \boldsymbol{u}_{ij}^e \tag{9}$$

where $\boldsymbol{u}^e(\mathbf{r})$ is the velocity in the mapped plane, $\mathbf{r} = (r, s)$ is the position in the mapped plane, N is the order of the Lagrange polynomial, l_i and l_j are Lagrange basis polynomials, and $\boldsymbol{u}_{ij}^e$ are the unknown basis coefficients.

The SEM is based on the concept of Lagrange polynomials (see Kreyszig [1]). Lagrange polynomials are often used to fit line to a number of data points. Given k points, the Lagrange polynomial fit to these points is

$$L(x) = \sum_{j=0}^{k} y_j l_j(x) \tag{10}$$

where L is y_j is the j-th given y value, and l_j is the j-th basis polynomial. The basis polynomials are defined as the product

$$l_j(x) = \prod_{\substack{0 \le m \le k \\ m \ne j}} \frac{x - x_m}{x_j - x_m} \tag{11}$$

The basis polynomials are defined such that $l_j(x_{m=j}) = 1$ and $l_j(x_{m \ne j}) = 0$. In a simple line fitting example, the y_j values are known. These y_j values can be thought of as weights applied to each basis polynomial. In the SEM case, the basis polynomials are set based on the mesh geometry and the desired Gauss-Lobatto-Legendre distribution, but the basis coefficients $\boldsymbol{u}_{ij}^{e}$ must be solved for by assembling a linear system of equations.

Equation (9) can be assembled for each element in the mesh. These equations are used to build the the linear system of equations along with the enforcement of boundary conditions and continuity between the elements. The linear system of equations is

$$A\underline{u} = Bf \tag{12}$$

where A is the global stiffness matrix, $\underline{u}$ is the vector of unknown basis coefficients, B is the global mass matrix, and f is the vector of forcing functions.

V. Final Problems

A. Solving Navier-Stokes for Couette Flow

The final task in devloping this 2D SEM code is to solve the full Navier-Stokes equation (7) in a few simple and well understood scenarios. The first situation is Couette flow as defined by Kundu et al. [2]. This case will consist of two parallel plates of length $l >> h$, where h is the distance between the plates. The upper plate will have some non-zero velocity, and the lower plate will have a velocity of zero, see the left hand side of Fig. 2.

To solve this problem, the domain, $l \times h$, will be split into n elements, and GLL points will be used to fit an N order polynomials to each element such that the SEM can be employed to solve Eq. (7), see the right hand side of Fig. 2. We plan to generate our own quadrilateral based meshes as this will be straightforward for the simple cases we plan on running.

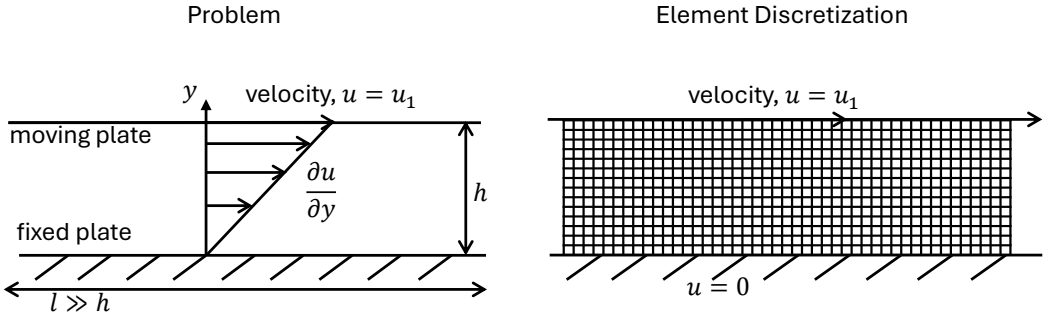

Fig. 2 Elemental Discretization of Couette Problem

B. Couette Flow

The final task in devloping this 2D SEM code is to solve the full Navier-Stokes equation (7) in a few simple and well understood scenarios. The first situation is Couette flow. This case will consist of two parallel plates of length $l >> h$,

where h is the distance between the plates. The upper plate will have some non-zero velocity, and the lower plate will have a velocity of zero, see the left hand side of Fig. 2.

To solve this problem, the domain, $l \times h$, will be split into n elements, and GLL points will be used to fit an N order polynomials to each element such that the SEM can be employed to solve Eq. (7), see the right hand side of Fig. 2.

C. Flow around an Airfoil

If time permits, we want to run some cases of flow around a $2-D$ airfoil as this could help guide some of our research endeavors after the conclusion of this course. For this problem we will employ a neumann condition which says that gradients in velocity at the farfield will be zero, $\frac{\partial u_i}{\partial x_i} = 0$, and we will also enforce a zero normal flow condition on the surface of the airfoil. The mesh will be generated using conformal mapping following the work by Kundu et al. [2], see Fig. 3. GLL points will again be used for the N-order polynomial fits.

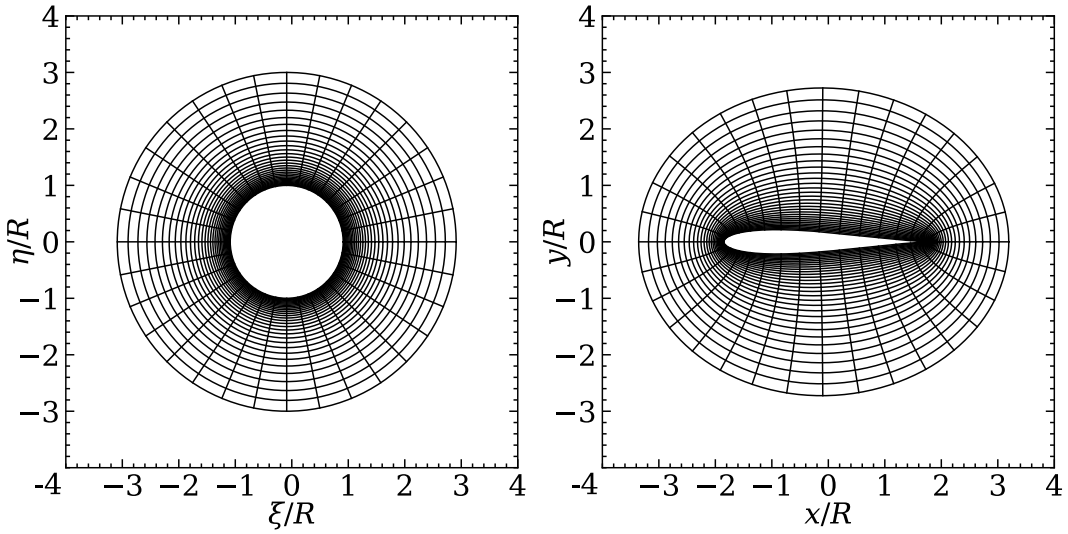

Fig. 3 Elemental discretization of airfoil problem. Adams used conformal mapping to generate the mesh on the right in terms of the mesh on the left.

VI. Conclusion

We expect the development of a rudimentary SEM code to be both challenging and informative. We hope to take what we learn from this project and apply it directly to our near future research endeavors.

References

[1] Kreysig, E., *Advanced Engineering Mathematics*, 8th ed., John Wiley & Sons, Inc., New York, 1999, Chap. 17, pp. 828–885.

[2] Kundu, P. K., Cohen, I. M., and Dowling, D. R., *Fluid Mechanics*, 6th ed., Academic Press, Massachusetts, 2015, Chap. 14, pp. 786–794.